Int J Adv Manuf Technol (2016) 85:2745–2759
DOI 10.1007/s00170-015-8079-x

ORIGINAL ARTICLE

Modeling and simulation of surface morphology abnormality of 'S' test piece machined by five-axis CNC machine tool

Zhong Jiang[1] · **Jiexiong Ding**[1] · **Zhiyong Song**[1,2] · **Li Du**[1] · **Wei Wang**[1]

Received: 31 July 2015 / Accepted: 3 November 2015 / Published online: 24 November 2015

Abstract In this paper, a convenient way to detect machining precision of five-axis CNC machine tool is suggested in theory. In a general way, NAS979 is cut to test machine tool; however, it fails to evaluate the combination motions of rotary axes sufficiently. Therefore, a novel S-shape test part, called 'S' test piece, has been presented to demonstrate the machine tool's capabilities. As a new test specimen, 'S' test piece has some advantage to exhibit the machining precision of five-axis machine tool. There are some visible marks related to performance of machine tool experimentally, however, the reasons for these abnormal marks are uncertain theoretically, the performance of the servo system may be one of the causes. In order to figure out the definite cause of the abnormal morphology, a simulated platform with the servo system is set up to amplify and the normal errors that come from the tracking of axes are presented. The simulation results of the abnormal morphology of 'S' test piece is provided. And the surface quality is evaluated by the peak-to-peak value (Vpp). There are obvious marks in four special regions of 'S' test piece that simulated with poor performance servo system, and these marks are invisible in the surface of 'S' test piece that simulated with good performance servo system. Vpp in these four regions changes greater than the other regions of 'S' test piece. The Vpp that simulated by the poor performance servo system is about 15 times larger than the error simulated by the optimized performance servo system in these four special regions. While, Vpp of other regions is essentially invariant. Then, the machining experiments of 'S' test piece are conducted with the standard suggested process. The abnormal morphology of machined 'S' test piece is so obvious that it can be observed by the naked eyes, without any test equipment. And the result of the experiment is consistent with the simulation result, which means that tracking errors of servo system have direct influence on surface morphology abnormality, and the surface quality of 'S' test piece could display the dynamic performance of the servo system intuitively in theory. As a standard comparison object, the surface quality of NAS979 test piece is analyzed through the same platform with the poor performance servo system, the largest Vpp is about 0.00022 mm, one eightieth smaller than 'S' test piece at least. And machining experiment is also carried out with the poor performance machine tool, the surface is so smooth that unexpected texture cannot be observed by the naked eyes, it should be test by the special measurements. The simulation results and experiment results both show that the surface quality of 'S' test piece is hugely worse than NAS979. Besides, there are several special regions of 'S' test piece to exhibit the surface texture waving with certain parameters. In a word, 'S' test piece is high effectively to exhibit the dynamic performance of the servo system of five-axis machine tool.

Keywords Five-axis CNC machine tool · Dynamic performance · Servo system · 'S' test piece · Surface morphology abnormality

✉ Jiexiong Ding
jxding@uestc.edu.cn

[1] School of Mechatronics Engineering, University of Electronic Science and Technology of China, Chengdu, China 611731

[2] CNC Machining Factory, Chengdu Aircraft Industrial (Group) Co. Ltd, Chengdu, China 610092

1 Introduction

The machine tool industry have developed rapidly in recent years, and there are tremendous demands in machine processing precision and quality, especially in the aerospace field [1]. The machining accuracy of CNC machine tools will directly

affect the performance of the processed products. Unknown precision of machine tool will lead to uncertain machining accuracy and surface quality. Hence, how to effectively exhibit the CNC machine tool error and effectively improve precision has become a very important and meaningful research field.

According to the references [2], there are four types of error sources that mainly influence the accuracy of machining surface, which are categorized as geometric error, control system error, thermal error, and deformation under cutting forces. For these error sources, there are two classical methods to detect the accuracy of CNC machine tools fast and efficiently. Firstly, special instrument is used to detect static error of machine tool. Secondly, standard specimen is cut to show dislocation. The common detection instruments are laser interferometer, Double Ball Bar (DBB), R-Test tester, etc. The method for measuring geometric error of CNC machine tool by DBB has been included in the revised edition of the international standard ISO 10791-6 [3]. Renishaw has developed a mature DBB product including the measurement equipment and software [4]. R-Tester will also be included in international standard as a new precision detection method of CNC machine tool. And IBS [5] and Fidia [6] have developed and commercialized a mature R-Test device.

All above detection instruments only can exhibit the static performance of the machine tool, that is, the detection is practicable unloaded. Thus, these methods can not accurately reflect the actual machining performance of machine tool. The machining precision of the machine tool is important to the machining quality of parts. Therefore, the acceptance of part precision becomes a key section in evaluating a machine tool. The best known part is NAS979 [7]. The geometry of NAS979 is a combination of a circle, a square, a diamond shape contour, and a 3°sided quadrilateral. Once a NAS979 part is machined, the results are used to define a series of measurements, such as square, parallelism, and circularity. NAS979 was developed in 1969 as a basis of the workpiece in ISO 10791-7. But it is seldom used to evaluate the coupled motion between two rotary axes or the combination of linear-rotary axes. Nowadays, many users demand high precision in 3D contouring application for a five-axis machine. A five-axis machine tool qualified by NAS979 often has some other machining problems such as unsmooth profile or poor surface quality at certain position as shown in Fig. 1. Since the demand for a five-axis machine is increasing rapidly, a test part or validation tests for this complex machine is essential.

Therefore, a novel S-shape test part, called ‘S’ test piece, has been presented to demonstrate the machine tool’s capabilities [8]. There are some successful applications in many fairs or showrooms. The new international standard test piece—‘S’ test piece was brought into ISO 10791-7 criterion group as an additional test piece in the 78th ISO conference in 2015. It shows some effect on dynamic precision detection of the machine tool experientially. However, the relationship between

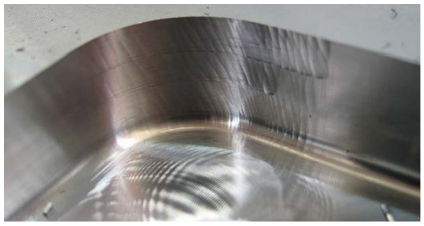

Fig. 1 The fault position of workpiece

the surface quality of ‘S’ test piece and the machine’s performances is still undiscovered theoretically.

For the research of the formation mechanism of surface morphology abnormality, some researchers suppose that the source of surface morphology abnormality is the unstable low-frequency milling chatter between the tool and workpiece. From the relationship analysis of the waviness interval and feed rate, Claryssea F and Vermeulena M pointed out that the frequency range is mainly limited to 10–50 Hz [9]. Many researchers have also investigated the machining dynamics about it, involving tool vibration model and cutting force model. Based on these models, some researchers focus on controlling spindle speed to decrease the milling chatter excited by transient cutting force [10, 11]. Some other researchers focus on controlling feed rate to suppress milling chatter [12–19].

The machining processes of ‘S’ test piece is a multi-segment processing along the sweeping line. There are eight machining layers. If the surface morphology comes from the vibration, the vibration amplitude, and phase of the eight layers is hardly the same, because the vibration is stochastic. The real surface of ‘S’ test piece is shown in Fig. 2. It is clearly that the wave profiles are substantially identical at every layer, which means the vibration may not be the main sources. Since the servo system has a good consistency during the same processes; therefore, the imperfection of the servo system may be one of the main sources.

In this paper, a simulation platform with servo system model and mechanical transmission model is set up. And the simulation of machining error caused by the servo system has been performed. Besides, some experimental tests have been completed to verify simulation. Finally, a comparative analysis between the NAS979 specimen and

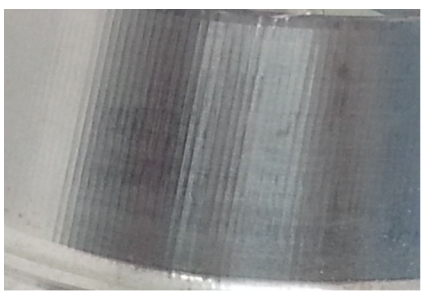

Fig. 2 The real surface of ‘S’ test piece

Table 1 (a) two sets of control points of ruled surface A

P	X	Y	Z	Q	X	Y	Z
P0	12	2.5	40	Q0	6	2.5	0
P1	21	57	40	Q1	9	57	0
P2	12	121	40	Q2	5	121	0
P3	27	176	40	Q3	25	185	0
P4	92	175	40	Q4	95	182	0
P5	123	142	40	Q5	130	145	0
P6	142	67	40	Q6	137	65	0
P7	170	18	40	Q7	168	10	0
P8	246	17	40	Q8	255	14	0
P9	259	85	40	Q9	262	85	0
P10	250	141	40	Q10	261	141	0
P11	258	197.5	40	Q11	264	197.5	0

Table 1 (b) two sets of control points of ruled surface B

M	X	Y	Z	N	X	Y	Z
M0	22	2.5	40	N0	16	2.5	0
M1	32	69	40	N1	19	69	0
M2	22	128	40	N2	15	128	0
M3	36	166	40	N3	35	174	0
M4	81	165	40	N4	81	172	0
M5	112	145	40	N5	120	149	0
M6	132	66	40	N6	126	63	0
M7	164	10	40	N7	160	3	0
M8	238	7	40	N8	243	1	0
M9	272	56	40	N9	275	52	0
M10	259	126	40	N10	270	125	0
M11	268	197.5	40	N11	274	197.5	0

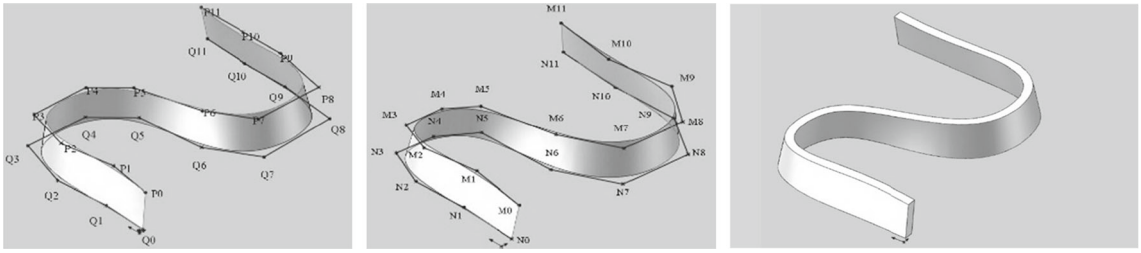

(a) (b) (c)

Fig. 3 Geometric definition of the test part. **a** Inner ruled surface A. **b** Outer ruled surface B. **c** Final shape

'S' test piece has been presented, and the comparative result shows that 'S' test part piece is valuable to exhibit the dynamic performance of servo system of five-axis machine tool clearly and intuitively.

2 The geometric feature of 'S' test piece

2.1 Geometric definition of 'S' test piece

The surfaces of 'S' test piece are modeled as follows. First, the boundary curve of S part is constructed, which is a three-order uniform rational B-spline curve. The equation of B-spline curve is expressed in Eq. (1).

$$Q(u) = \sum_{i=0}^{n} P_i N_{i,m}(u) \tag{1}$$

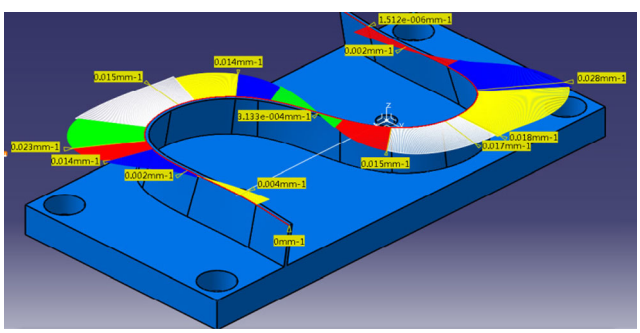

Fig. 4 Variable curvature on upper boundary line

Where, $P_i(i=0,1,\cdots,n)$ and $N_{i,m}(u)$ are the control points and the base function affecting the shape of curve respectively. m is the order of spline curve. The base function references to the De Boor-Cox method [20]. Each segment is composed with four control points and has four base functions. The base functions on the first two segments and the last two segments are different. The other segments have the same one. They are expressed as Eqs. (2)–(6),

The first segment,

$$\begin{cases} N_{1,3}(u) = -u^3 + 3u^2 - 3u + 1 \\ N_{2,3}(u) = \frac{7}{4}u^3 - \frac{9}{2}u^2 + 3u \\ N_{3,3}(u) = -\frac{11}{12}u^3 + \frac{3}{2}u^2 \\ N_{4,3}(u) = \frac{1}{6}u^3 \end{cases} \tag{2}$$

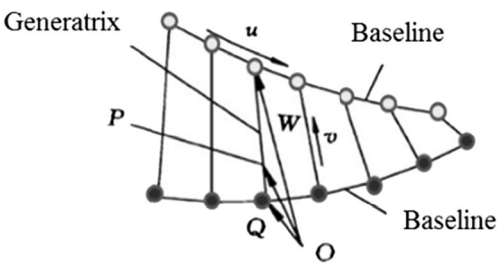

Fig. 5 The ruled surface diagram

The second segment,

$$\begin{cases} N_{1,3}(u) = -\frac{1}{4}\left(u^3 + 3u^2 - 3u + 1\right) \\ N_{2,3}(u) = \frac{1}{12}\left(7u^3 - 15u^2 + 3u + 7\right) \\ N_{3,3}(u) = -\frac{1}{6}\left(3u^3 - 3u^2 - 3u + 1\right) \\ N_{4,3}(u) = \frac{1}{6}u^3 \end{cases} \tag{3}$$

The third to n-1 segment,

$$\begin{cases} N_{1,3}(u) = \frac{1}{6}(1-u)^3 \\ N_{2,3}(u) = \frac{1}{6}\left(3u^3 - 6u^2 + 4\right) \\ N_{3,3}(u) = \frac{1}{6}\left(-3u^3 + 3u^2 + 3u + 1\right) \\ N_{4,3}(u) = \frac{1}{6}u^3 \end{cases} \tag{4}$$

The last but one segment,

$$\begin{cases} N_{1,3}(u) = -\frac{1}{6}\left(u^3 - 3u^2 + 3u - 1\right) \\ N_{2,3}(u) = \frac{1}{2}u^3 - u^2 + \frac{2}{3} \\ N_{3,3}(u) = -\frac{1}{12}\left(7u^3 - 6u^2 - 6u - 2\right) \\ N_{4,3}(u) = \frac{1}{4}u^3 \end{cases} \tag{5}$$

The last segment,

$$\begin{cases} N_{1,3}(u) = -\frac{1}{6}\left(u^3 - 3u^2 + 3u - 1\right) \\ N_{2,3}(u) = \frac{1}{12}\left(11u^3 - 15u^2 - 3u + 7\right) \\ N_{3,3}(u) = -\frac{1}{4}\left(7u^3 - 3u^2 - 3u - 1\right) \\ N_{4,3}(u) = u^3 \end{cases} \tag{6}$$

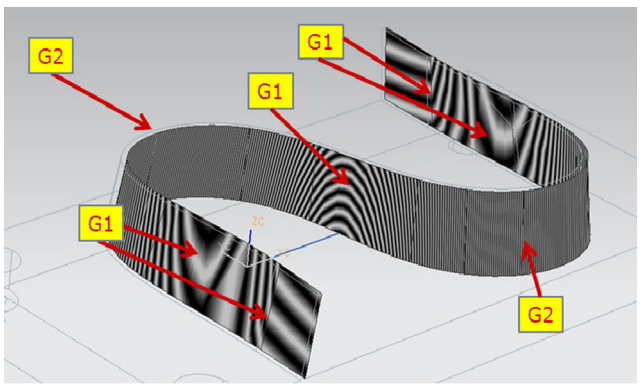

Fig. 6 Normal curvature of 'S' test piece

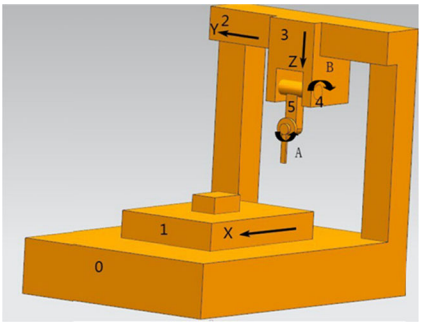

Fig. 7 Model of five-axis machine tool

Two sets of control points *Pi* and *Qi* are given in Table 1 (a). Thus, two boundary B-spline curves are created by these sets of points. The inner surface of S part is composed by sweeping the bus bar along the boundary curves, as shown in Fig. 3a.

Second, another two sets of points *Mi* and *Ni* are shown in Table 1 (b). Similarly, the outer surface of S part is composed as shown in Fig. 3b. Finally, two ruler surfaces are constructed into S part as shown in Fig. 3c.

2.2 The geometric characteristics of 'S' test piece

Suppose that the curve $L: u=u(t), v=v(t)$, is a curve through the point $P_0(u_0, v_0)$ on 'S' test piece, the equation of curve L can be got as

$$\boldsymbol{r} = \boldsymbol{r}(u(t), v(t)) \tag{7}$$

So the tangent line of curve L at point $P_0(u_0, v_0)$ is

$$r'\Big|_{t_0} = \boldsymbol{r}_u(u_0, v_0)\left(\frac{du}{dt}\right)\Big|_{t_0} + \boldsymbol{r}_v(u_0, v_0)\left(\frac{dv}{dt}\right)\Big|_{t_0} \tag{8}$$

The curvature of curve L at point $P_0(u_0, v_0)$ is expressed as Eq. (9):

$$k = \frac{\left|r' \times r''\right|}{\left|r'\right|^3} \tag{9}$$

Figure 4 shows various curvatures in up boundary curve. In the beginning, the curvature is very small, approximately as a

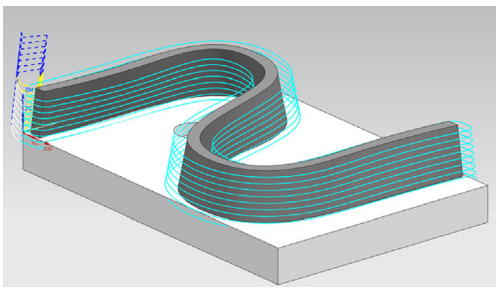

Fig. 8 Machining tool paths of 'S' test piece

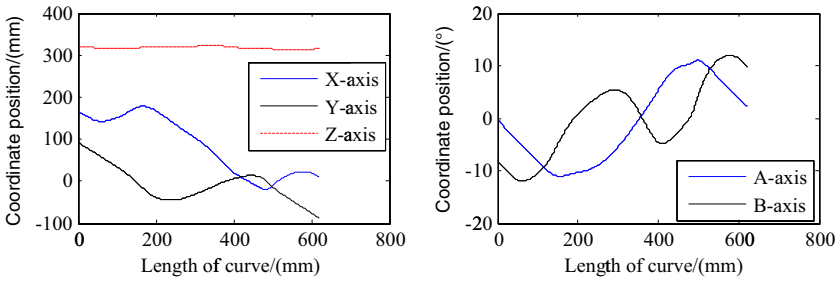

Fig. 9 Commands of machining 'S' test piece. **a** Commands of *X*-, *Y*-, and *Z*-axis. **b** Commands of *A*- and *B*-axis

straight line. Then the curvature changes its bending direction and increases quickly. After passing the maximum circle, the curvature gradually decrease. Subsequently, the curvature reverses the bending direction again at the cross-point of two boundary projection curve. The curvature plot at right side is the mirror symmetry through the cross-point. With so many arcs pieced together, 'S' test piece can show the machining performances as a complex surface with rapid change of curvature.

Curvature continuity is another important feature of a ruled surface. The boundary curve of 'S' test piece is a three-order B-spline curve, which means the curve has two order continuity, geometric continuity, tangent continuity, and curvature continuity. However, it does not mean the surface has the corresponding continuity, which needs to satisfy the continuity along every possible curve. Usually, the normal curvatures of the surface are calculated to show the changes at different directions. As shown in Fig. 5, the ruled surface vector equation is expressed as Eq. (10):

$$r(u,v) = a(u) + vb(u) \tag{10}$$

Where $a{=}a(u)$ is the movement traverse line, v is running parameter of the generatrix which its unit vector is $b(u)$. The vector equation of the ruled surface is modeled as Eq. (11):

$$\begin{cases} r_u = a'(u) + vb'(u) \\ r_v = b(u) \\ r_{uu} = a''(u) + vb''(u) \\ r_{uv} = b'(u) \\ r_{vv} = 0 \end{cases} \tag{11}$$

Then, the unit normal vector of certain point on the twisted ruled surface is represented as Eq. (12).

$$n = \frac{r_u \times r_v}{\sqrt{EG{-}F^2}} = \frac{a' \times b + vb' \times b}{\sqrt{EG{-}F^2}} \tag{12}$$

Where, E,F,G is the first basic scalar function respectively, they can be calculated as Eq. (13).

$$\begin{cases} E = {r_u}^2 = (a' + vb')^2 \\ F = r_u r_v = (a' + vb')b \\ G = {r_v}^2 = b^2 \end{cases} \tag{13}$$

Similarly, the ruled surface second fundamental equation can be obtained by the Eq. (14).

$$\begin{cases} L = nr_{uu} = \dfrac{a' \times b + vb' \times b}{\sqrt{EG{-}F^2}}[a'' + vb''] \\ M = nr_{uv} = \dfrac{(a' \times b)\cdot b'}{\sqrt{EG{-}F^2}} = \dfrac{(a', b, b')}{\sqrt{EG{-}F^2}} \\ N = r_{vv} n = 0 \end{cases} \tag{14}$$

The principal curvatures k_i on the ruled surface anywhere can be gained by the Eq. (15):

$$\left(EG{-}F^2\right){k_i}^2{-}(EN{-}2FM + GL)k_i + \left(LN{-}M^2\right) = 0 \tag{15}$$

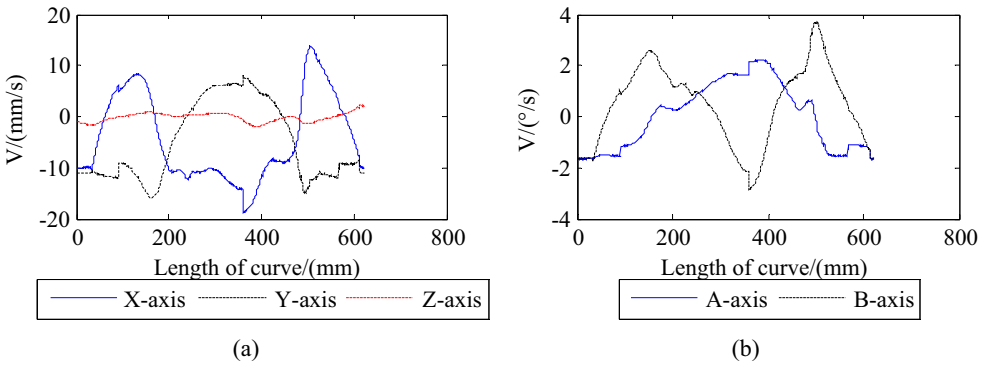

Fig. 10 Velocity of each axis. **a** Translation axis velocity. **b** Rotary axis velocity

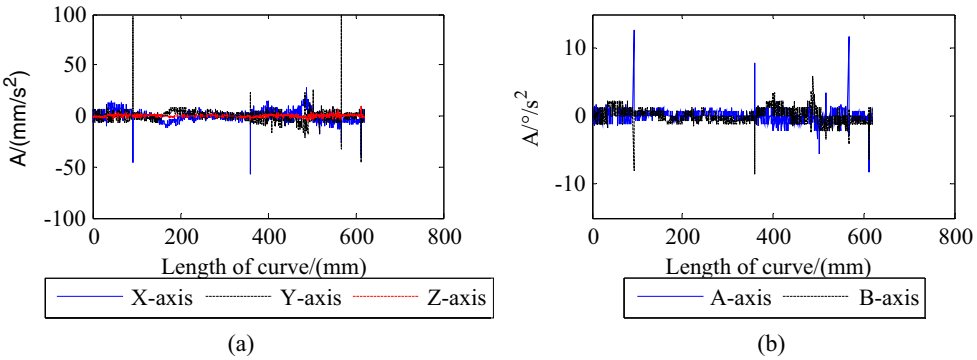

Fig. 11 Acceleration of each axis. **a** Translation axis acceleration. **b** Rotary axis acceleration

The two main directions of g_1 and g_2 corresponding to the main curvature are as Eq. (16)

$$\begin{cases} g_1 = \dfrac{du}{dv} = \dfrac{k_1 F - M}{L - k_1 E} \\ g_2 = \dfrac{du}{dv} = \dfrac{k_2 G - N}{M - k_2 F} \end{cases} \tag{16}$$

Where, k_1, k_2 is the first main curvature and the second main curvature, respectively.

Then, the normal curvatures of the surface k_n can be expressed as,

$$k_n = k_1 \cos^2\varphi + k_2 \sin^2\varphi \tag{17}$$

Where, φ is the angle between the principle direction and any tangent direction. Substituting the include angle from 0 to 2π, the normal curvature along different curves may be calculated. Another way to exhibit the continuous area is the Isolux. Choosing a light projected on S part surface, the strips on surface could display the continuity. If the strips change the shape or jump sideway as they cross the connection, there is geometric discontinuity G0 at the surface. If the stripes go cross the connection but turn sharply, there is tangent discontinuity G1. If the stripes match and continuously go smoothly over the connection, there is curvature discontinuity G2. The Isolux figure of 'S' test piece is shown in Fig. 6. The strips at the first and last area turn sharply, where G1 continuity exists. The most of area on 'S' test piece has the same finest strips, where G2 continuity is exhibited.

2.3 Kinematic characteristic in machining 'S' test piece

In order to figure out the kinematic characteristic in machining 'S' test piece, 'S' test piece model is input into CAM software such as UG and CATIA. The type of five-axis machine tool is selected. Then, the post processing file including the position of each axis, the feed rate, and the spindle speed is given by the CAM software. In this paper, the type of machine tool with two rotary axes in the spindle head is taken as an example. The machine tool model is shown as Fig. 7. The structural code can be described as [w X b Y Z B A(C) t] by connecting the motion axes from the workpiece side to the tool side. In this description, the workpiece side and the tool side are distinguished by naming the workpiece by 'w', the tool by 't', and the bed by 'b'; (C) stands for the spindle axis without numerical control for angular positioning.

The machining processes of 'S' test piece is a multi-segment processing along the sweeping line, and there are eight machining layers. The machining tool paths of 'S' test piece are shown in Fig. 8.

The tool paths of each machining layer are very similar. The motion commands of one layer are shown in Fig. 9.

From Fig. 9, the motions of all axes except *Z*-axis change during the machining, and the motion of each axis changes in a non-linear way. Thus, all axes will not have a constant speed during the machining. Furthermore, each axis reverses the direction for several times, for example three times for *A*-axis and four times for *B*-axis. As we all know, the motion

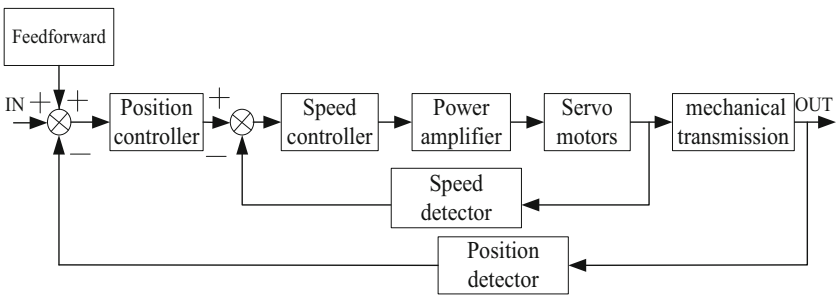

Fig. 12 Servo system block diagram

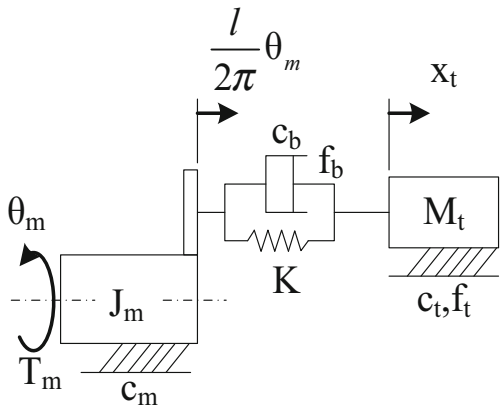

Fig. 13 Dynamic model of translational axis

direction reverses of axis will lead to a larger tracking error. Therefore, the multi-reverse will bring strong effect on dynamic error.

Assuming the tool moves from one point $P_1(X_1, Y_1, Z_1, A_1, B_1)$ to another point $P_2(X_2, Y2, Z_2, A_2, B_2)$, the feed rate is V. In a very short time, the speed of feed can be considered as a constant. So the moving time ΔT_1 is

$$\Delta T_1 = (P_2 - P_1)/V \tag{18}$$

During the process, five axes coupled move and have the same moving time. In a short moving time, the axis speed can also be assumed to be constant. Thus, the ideal speed of each axis can be calculated by the displacement dividing the time, as follows:

$$\begin{cases} V_{x1} = (X_2 - X_1)/\Delta T_1 \\ V_{y1} = (Y_2 - Y_1)/\Delta T_1 \\ V_{z1} = (Z_2 - Z_1)/\Delta T_1 \\ V_{A1} = (A_2 - A_1)/\Delta T_1 \\ V_{B1} = (B_2 - B_1)/\Delta T_1 \end{cases} \tag{19}$$

When the feed rate is 1200 mm/min, the velocity of each axis is shown in Fig. 10. The acceleration can also be calculated by the speed difference dividing the moving time again in Fig. 11. Except Z-axis, all axis speed has an irregular fluctuation. The difference between the peak and the bottom is obvious. It requires the machine tool has a good acceleration and deceleration ability. The poor acceleration and deceleration ability of machine tool will lead to the motion response delay, which causes the contour error of workpiece larger. On the other hand, S part would easily show the poor surface quality if the machine center does not have a good dynamic performance at certain position.

3 Cutting simulation modeling for 'S' test piece

3.1 Cutting simulation model of machine tool

For a five-axis machine tool, each axis has an independent servo and mechanical system. The system on the linear axis or the rotary axis has the similar control diagram including the position loop, the velocity loop, the motor loop, and the mechanic structure, seen in Fig. 12 [9]. Furthermore, the feedforward loop is added to the servo system for greater accuracy.

Inputting the commands of each axis, the actual position would be off the ideal position that is called tracking error due to the hysteresis effect of each axis. The error can be simply expressed as Eq. (20), which indicates that the tracking error is proportional to the speed of axis and inversely proportional to the position gain K_{pp}. Based on this principle, decreasing the speed while increasing the position gain would significantly reduce the tracking error. However, decreasing speed would lead to low machining efficiency, and too large position gain may causes system instability. Therefore, there must be a compromise, reasonable parameters of servo system. In order to describe the dynamic behavior of the machine tool accurately, it is necessary to set up the whole model.

$$e = X_{\text{ideal}} - X_{\text{real}} \approx \frac{V(X, Y, Z, A, B)}{K_{pp}} \tag{20}$$

The translational axis is driven by the motor, where the ball screw is used to transform the rotate movement to the rectilinear motion. The mechanical system includes the motor, ball screw, the workbench, and the guide, seen in Fig. 13. The structure component is consist of the motor torque, the friction, the damping, and inertia force between bodies. There are two degrees of freedom as shown in Fig. 13, the rotating motor and the moving workbench. The dynamic equations

Table 1 Meaning of symbols in dynamic equations of translational axis

Symbol	Physical meaning	Symbol	Physical meaning
J_m	Moment of inertia of the motor	T_m	Torque of the motor
θ_m	Rotation angle of the motor	c_m	The damping coefficient of the motor
K	Equivalent axial stiffness	c_b	Damping coefficient of ball screw
l	Screw lead	f_b	Friction torque of ball screw
M_t	Equivalent mass of workbench	x_t	Displacement of the translation axis
c_t	Damping coefficient of guide	f_t	Friction of the guide

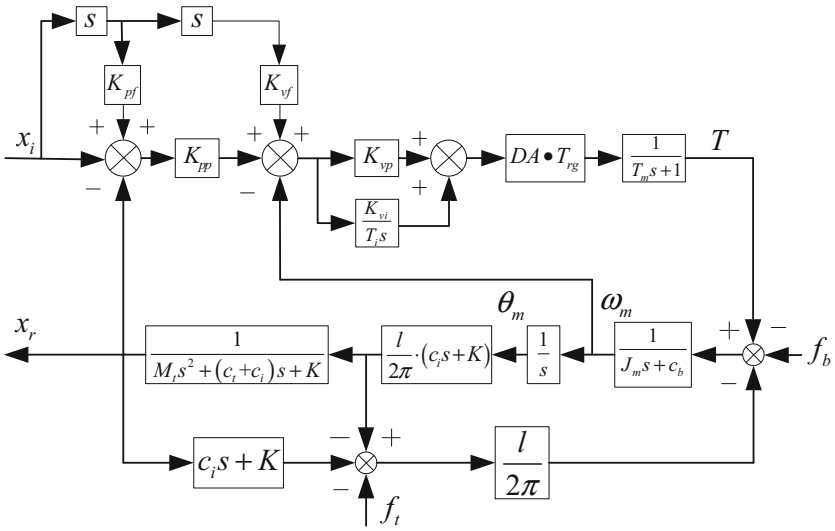

Fig. 14 Simulation model of servo system for the translation axis

are expressed as Eq. (21) and Eq. (22). The meaning of symbols is shown in Table 1.

$$J_m\ddot{\theta}_m + c_b\dot{\theta}_m + f_b + \frac{l}{2\pi}K\left(\frac{l}{2\pi}\theta_m - x_t\right) + \frac{l}{2\pi}c_i\left(\frac{l}{2\pi}\dot{\theta}_m - \dot{x}_t\right) = T_m \quad (21)$$

$$M_t\ddot{x}_t + c_t\dot{x}_t + f_t = \frac{l}{2\pi}K\left(\frac{l}{2\pi}\theta_m - x_t\right) + \frac{l}{2\pi}c_i\left(\frac{l}{2\pi}\dot{\theta}_m - \dot{x}_t\right) \quad (22)$$

So the transfer functions of mechanical system can be obtained by taking the Laplace transformation on the above dynamic equations. Other loops, such as position loop and velocity loop can describe with classical functions [21, 22]. In a word, the whole servo control system of the translational axis can be expressed in Fig. 14.

The output of rotary axis is the angular displacement. In the mechanical system, the worm gear transform is used to connect the motor to the workbench. There are three degree of freedoms, the rotating motor, the rotating worm gear, and the rotating workbench, seen in Fig. 15. The dynamic equations are expressed as Eq.(23)–Eq.(25). The meaning of symbols is shown in Table 2.

$$J_m\ddot{\theta}_m + C_m\dot{\theta}_m + R_g C_{ig}\left(R_g\dot{\theta}_m - \dot{\theta}_w\right) + f_m = T_m \quad (23)$$

$$J_w\ddot{\theta}_w + C_w\dot{\theta}_w + R_w C_{iw}\left(R_w\dot{\theta}_w - \dot{\theta}_t\right) + f_w = T_w + C_{ig}\left(R_g\dot{\theta}_m - \dot{\theta}_w\right) \quad (24)$$

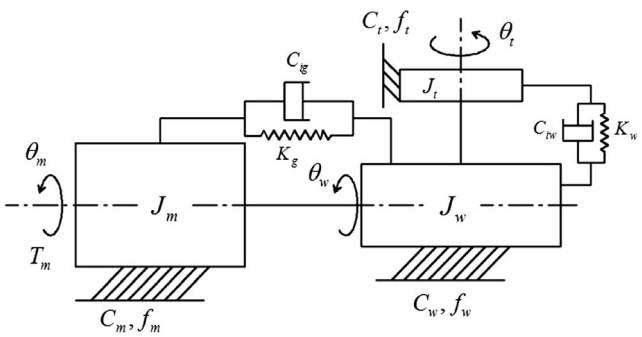

Fig. 15 Dynamical model of rotary axis

$$J_t\ddot{\theta}_t + C_t\dot{\theta}_t + f_t = T_w + C_{iw}\left(R_w\dot{\theta}_w - \dot{\theta}_t\right) \quad (25)$$

In a similar way, by coupling the position loop, velocity loop, and the mechanical system together, the whole servo control system of the rotary axis is expressed in Fig. 16.

After the commands are input to the simulation model of servo system, the tracking error of each axis would be simulated as shown in Fig. 17. It is obvious that the tracking error graph of each axis is similar to the axis velocity, it is verified that the tracking error is proportional to the speed of axis.

Each driving movement of the machine tool cannot eliminate the tracking error due to the servo controller dynamics. In Fig. 18, P_{ideal} is a command position in two-axis machine tool. P_{real} is the actual position delivered by CNC unit. The tracking errors $\Delta x, \Delta y$ exist on two axes independently. These errors are transformed to the tool tip, resulting in tool center point (TCP) errors e between the ideal tool path and actual path. So the tracking error of each axis cannot represent the TCP errors. Therefore, it is necessary to integrate the tracking error of each axis to tool center point.

The tracking error of each axis is defined as ($\Delta X, \Delta Y, \Delta Z, \Delta A, \Delta B$), and ($X_{\text{axis\_}i}, Y_{\text{axis\_}i}, Z_{\text{axis\_}i}, A_{\text{axis\_}i}, B_{\text{axis\_}i}$) is defined as the ideal commands of each axis. The transformation principle between the tool center point and the rotate center point is shown in Fig. 19. The length between the tool center point and the rotate center point is L. From Fig. 19, the practical trajectory ($X_{\text{Tool\_}r}, Y_{\text{Tool\_}r}, Z_{\text{Tool\_}r}, A_{\text{Tool\_}r}, B_{\text{Tool\_}r}$) can be calculated in method of coordinate transformation as shown in Eq. (26). With the compensation of tool radius, the practical contour of 'S' test piece is achieved.

$$\begin{cases} X_{\text{Tool\_}r} = (X_{\text{axis\_}i} + \Delta X) - L\cdot[\cos(A_{\text{axis\_}i} + \Delta A)\cdot\sin(B_{\text{axis\_}i} + \Delta B)] \\ Y_{\text{Tool\_}r} = (Y_{\text{axis\_}i} + \Delta Y) + L\cdot[\sin(A_{\text{axis\_}i} + \Delta A)] \\ Z_{\text{Tool\_}r} = (Z_{\text{axis\_}i} + \Delta Z) - L\cdot[\cos(A_{\text{axis\_}i} + \Delta A)\cdot\sin(B_{\text{axis\_}i} + \Delta B)] \end{cases} \quad (26)$$

Table 2 Meaning of symbols of rotation axis

Symbol	Physical meaning	Symbol	Physical meaning
J_m	Moment of inertia of the motor	θ_m	Angular displacement of the motor
C_m	Damping coefficient of the motor	R_g	Gear ratio
T_g	Output torque of gear transmission	C_{ig}	Damping coefficient of between motor and gear transmission
f_m	Friction torque of the motor	T_m	Output torque of the motor
J_w	Moment of inertia of worm gear	θ_w	Angular displacement of worm gear
C_w	Damping coefficient of worm gear	R_w	Worm gear ratio
C_{iw}	Damping coefficient between the workbench and worm gear	J_t	Moment of inertia of workbench
θ_t	Angular displacement of workbench	C_t	Damping coefficient of workbench
f_t	Friction torque of workbench	T_w	Output torque of workbench

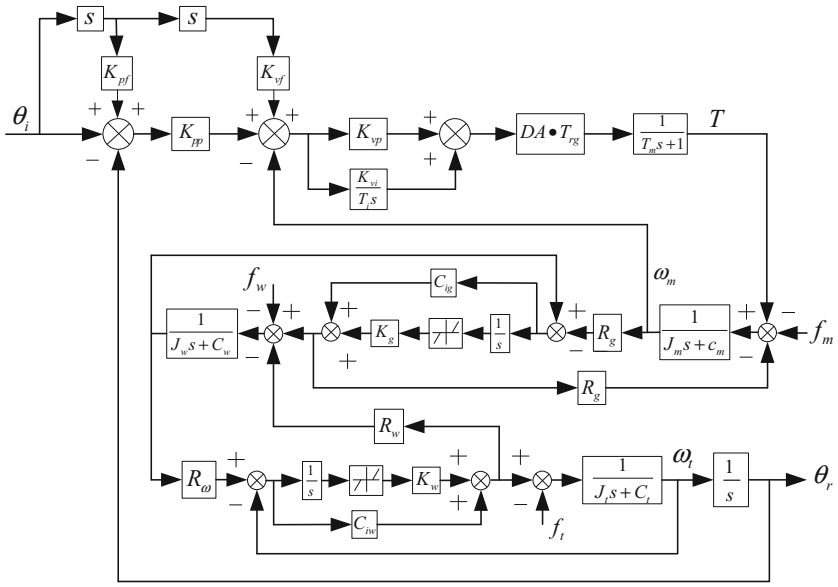

Fig. 16 Simulation model of servo system for rotation axis

3.2 Error process to exhibit waves of 'S' test piece

The actual contour can be simulated in the aforementioned simulation model, thus, the contour error can be calculated by comparing with the ideal contour defined by geometric. And the contour error would be expressed as the profile error, waviness, and roughness after error combination. Since profile error is always much larger than the other two surface texture, the real surface quality may not be presented cleanly. Therefore, it is necessary to

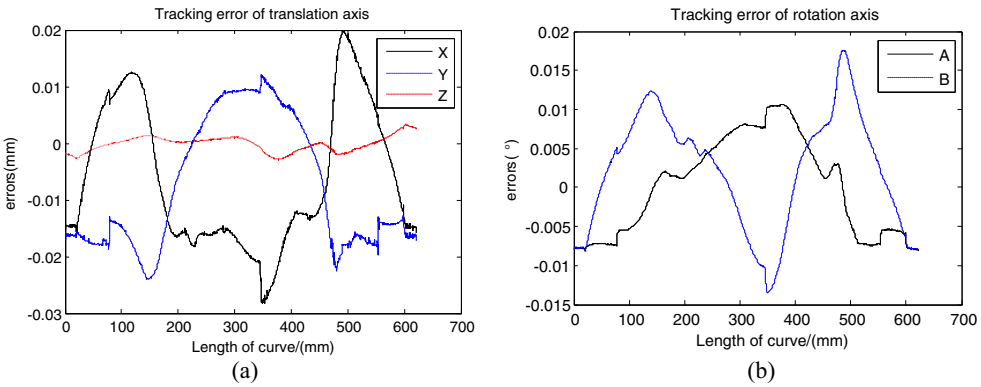

Fig. 17 Tracking errors of each axis. **a** Tracking errors of translation axis. **b** Tracking errors of rotary axis

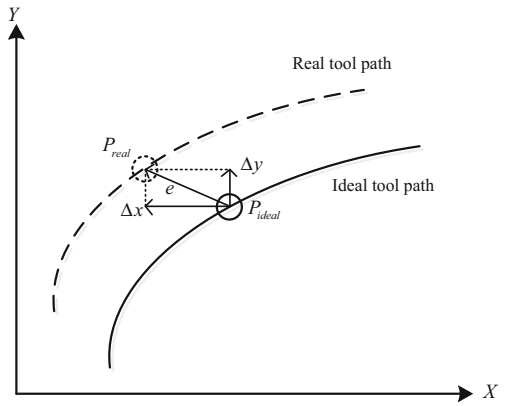

Fig. 18 Tracking errors of the commands

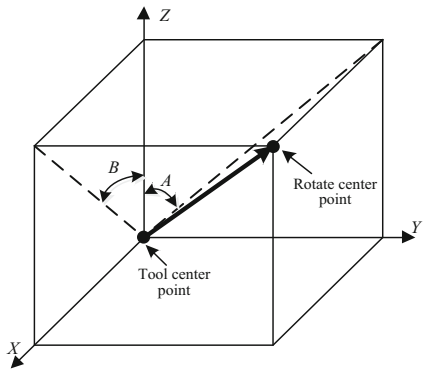

Fig. 19 The transformation principle graph

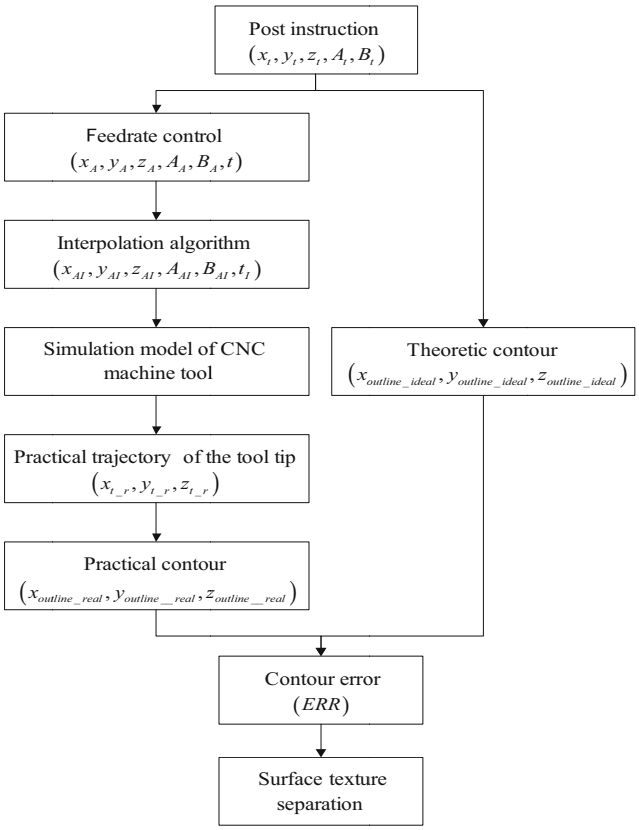

Fig. 21 Simulation flow of the servo system

pick up the real surface information from the workpiece profile.

The filtering method has been provided in the international standard ISO 12085:1996[23] to pick up the useful surface information. High pass filter method is widely used to remove the trend of the error curve. As an example, there is a profile error shown as the solid line in Fig. 20a. It is a similar parabola line with fluctuations. It is clear that the fluctuations are much smaller than the trend curve of the profile error. If the error is only expressed by the original error like the solid line in Fig. 20a, there may be one large mark on the surface; thus, many details that are more likely to be the surface problem may be ignored. Comparing with the trend curve of the profile error, the fluctuations are the high frequency components. Thus, a high pass filter is used to pick up the useful surface information, and the high frequency components are shown in Fig. 20b. Since the detail information of 'S' test piece surface is the major concern, high pass components is adopted to exhibit the surface quality of workpieces.

4 Simulation

4.1 Simulation of error on 'S' test piece

In order to ensure the similarity of the simulation and the practical machining, simulation flow is planned according to the machining flow of 'S' test piece.

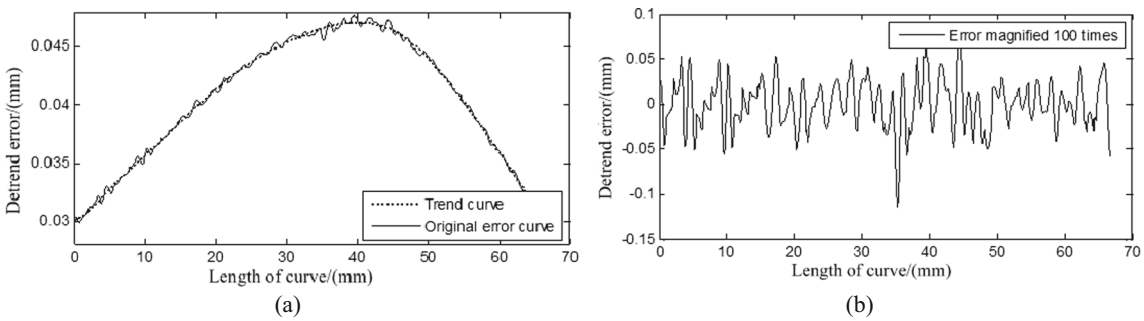

Fig. 20 Error-filtering result diagram. **a** Original error and trend curve. **b** High frequency components

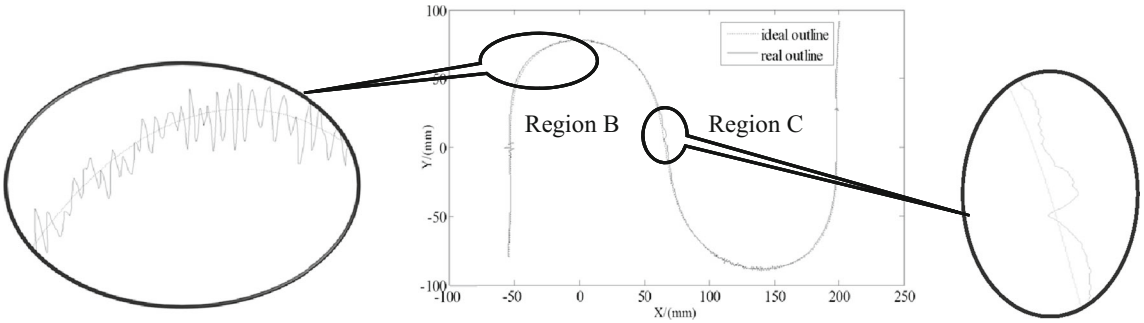

Fig. 22 Simulated contour of 'S' test piece

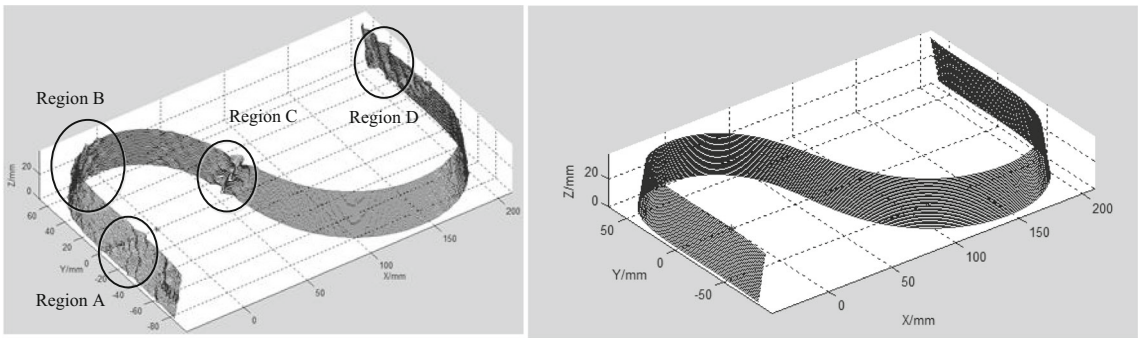

Fig. 23 Simulated surface of 'S' test piece machined by different performance machine tool **a** Machined by poor performance machine tool. **b** Machined by optimized performance machine tool

Table 3 The peak-to-peak value (Vpp) of 'S' test piece (millimeter)

'S' test piece	Region A	Region B	Region C	Region D	Other regions
Poor performance	0.0055	0.0075	0.0184	0.0094	0.0019
Optimized performance	0.0006	0.0063	0.0008	0.0008	0.0016

As shown in Fig. 21, the contour error can be calculated with five steps: First, the coordinate of the tool tip is fetched from the NC post instruction, and the coordinate is transformed into positional instruction of each axis. Second, the practical cutting speed and runtime of instruction is calculated with the S-shaped acceleration and deceleration algorithm. Then, the positional instruction of each axis is recalculated through linear interpolation algorithm. After that, the practical trajectory of the tool tip can be calculated by simulating with the recalculated positional instruction and the simulation model of the servo systems. Then, the contour error is calculated by comparing the ideal contour and the contour calculated from the simulation trajectory. Finally, the high frequency components are obtained by separating surface texture.

According to the simulation flow proposed above, simulation of one layer of 'S' test piece has been carried out. The contour error is obtained, and the high frequency components are obtained by separating in band. In order to express the error information effectively, these high frequency components are magnified 50 times and added to the ideal outline as continuous line in Fig. 22. The ideal contour is expressed as dashed line.

In Fig. 22, it is clearly that there are obvious ripples at the arc part and obvious tool marks at the middle area of 'S' test piece. In order to verify that the performance of servo system is the main error sources, which cause the wave profiles that are substantially identical at every layers, the simulation with

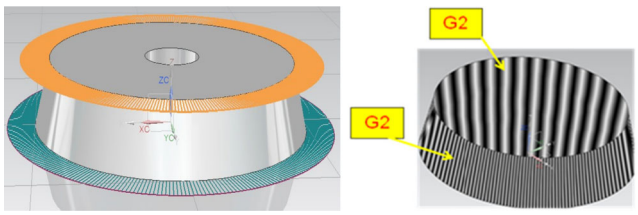

Fig. 24 Geometric characters of NAS979 test piece. **a** Curvature of NAS979 test piece. **b** Normal curvature of NAS979 test piece

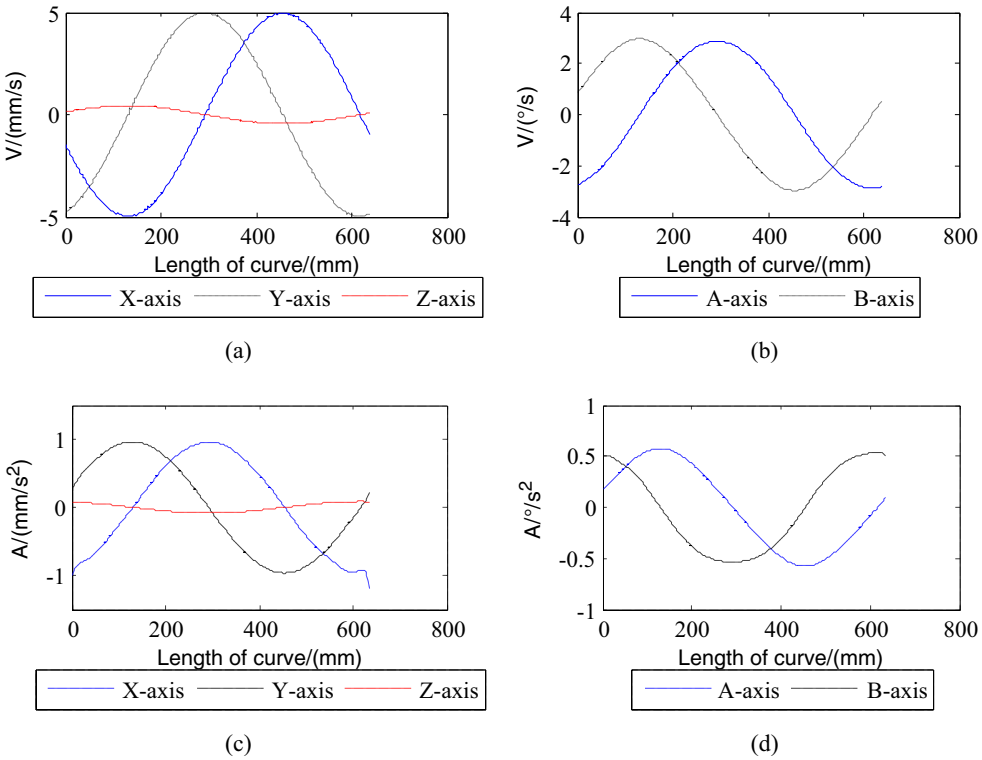

Fig. 25 Motion characters of NAS979 test piece. **a** Translation axis velocity. **b** Rotary axis velocity. **c** Translation axis acceleration. **d** Rotary axis acceleration

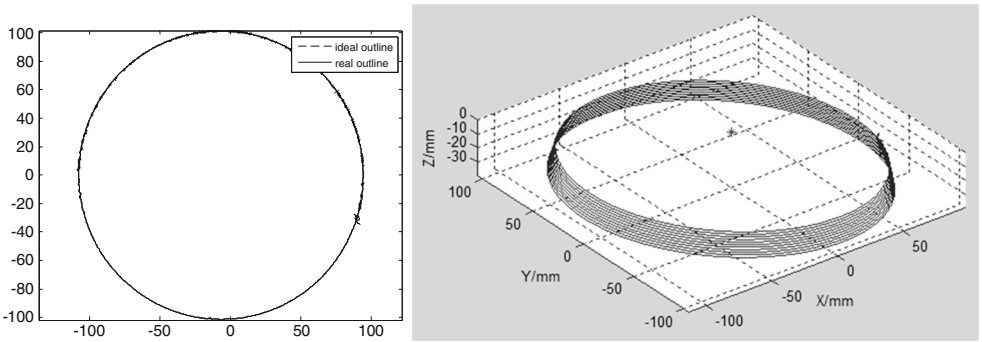

Fig. 26 Simulated result of NAS979 test piece machined by poor performance machine tool. **a** Simulated contour of one layer of NAS979. **b** Simulated surface of NAS979 test piece

the input of every layer of the finish machining NC instruction of 'S' test piece has been carried out. And each high frequency components of every layer is magnified 50 times. The simulation result is shown in Fig. 23a.

Figure 23a shows that the surface of each layer is similar. There are obvious ripples at the circular part and obvious tool marks at the middle area of 'S' test piece. Besides, there are obvious ripples at the beginning part and ending part of 'S' test piece. These four regions are named as regions A–D as shown in Fig. 23a. If the parameters of servo system are optimized, the surface quality of 'S' test piece is shown in Fig. 23b. The error is also magnified 50 times. The simulation surface obtained by the optimized performance of servo system is far smoother than the poor performance one. Since the error in these four regions are ripples, the peak-to-peak value (Vpp) is used to characterize the surface quality. The Vpps of four regions of two 'S' test pieces shown in Fig. 23 are

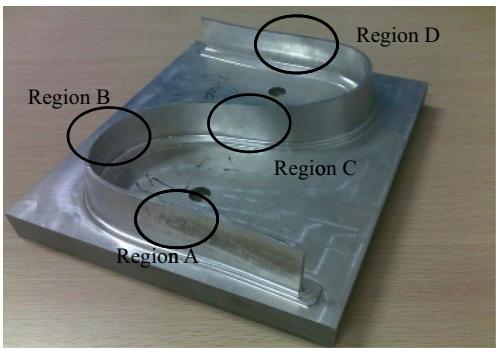

Fig. 27 The finished 'S' test piece

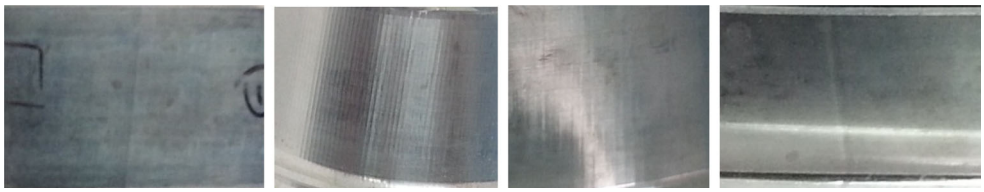

(a) (b) (c) (d)

Fig. 28 Surface quality of 'S' test piece machined by poor performance machine tool. **a** Region A. **b**. Region B. **c** Region C. **d** Region D

calculated as shown in Table 3. Comparing with other regions, Vpp in regions A–D increases with performance of servo system worse. Therefore, the performance of servo system is the main error sources of surface quality of 'S' test piece, which cause the wave profiles that are substantially identical at every machining layers.

Actually, these phenomenon are caused by the geometric characters of 'S' test piece. From Fig. 4, the curvature of region A, C, and D all cross the zero point, and there is a peak in region B, which would cause the motion and velocity of each axis change rapidly. From Fig. 6, the normal curvature of region A, C, and D are all G1 continuity. When machining these connection areas, the position and orientation of cutting tool would dramatically change as shown in Figs. 9, 10, and 11, which would cause the larger tracking error. Eventually, these characters lead to the synchronous motion performance of five axes deteriorates and there is the poor surface quality. In other words, the variation of surface quality of 'S' test piece could exhibit the dynamic performance of the machine tool.

4.2 Comparing 'S' test piece with NAS979

Up to now, the most popular test part for five-axis machine center is NAS979. Thus, the superiority of 'S' test piece would be found by comparing with NAS979.

The geometric characters and motion characters of NAS979 is shown in Figs. 24 and 25.

From Fig. 24, curvature in boundary line of NAS979 is constant, and the surface of NAS979 is G2 continuity. From Fig. 25, the velocity and accelerated acceleration is much smoother than 'S' test piece. Therefore, NAS979 may be easier to be machined than 'S' test piece.

Then, the simulation of NAS979 test piece using the poor performance servo system has been carried out. The simulation outline of NAS979 is shown in Fig. 26. In Fig. 26a, the high pass component is also magnified 50 times and added to the ideal outline to display, the ideal outline is expressed as dashed line and the calculated outline is expressed as solid line. The real outline is almost the same, and the high pass component is very small. The simulation results with the input of all layers are shown in Fig. 26b. The results show that the error of each layer is the same small. The simulation outline of NAS979 is smoother than the outline of 'S' test piece, and the largest peak-to-peak value (Vpp) is about 0.00022 mm, one eightieth smaller than the value of 'S' test piece machined by poor performance at least. So, it may be difficult to observe the error without the special equipment.

Based on comparative analysis of 'S' test piece and NAS979, it is obviously to result that the surface texture of the 'S' test piece could exhibit the dynamic performance of the servo system than NAS979 more directly.

5 Experiments

In order to verify the above results of the simulation and analysis, the cutting experiments of S part are carried out on two five-axis machine tools with different performance. The machined workpiece is shown in Fig. 27, and the surface quality in regions A–D machined by the poor performance and improved performance is shown in Figs. 28 and 29, respectively.

It is obvious that the surface quality machined by the improved performance machine tool is better than the poor performance. The difference in machining surface may be confirmed without the special equipment, because it can be observed by the naked eyes. The comparison result of the experiment is consistent with the simulation result, which means that performance of servo system has direct influence on surface morphology abnormality.

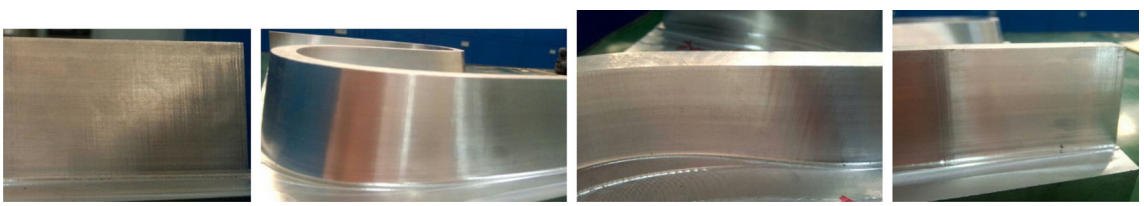

(a) (b) (c) (d)

Fig. 29 Surface quality of 'S' test piece machined by improved performance machine tool. **a** Region A. **b** Region B. **c** Region C. **d** Region D

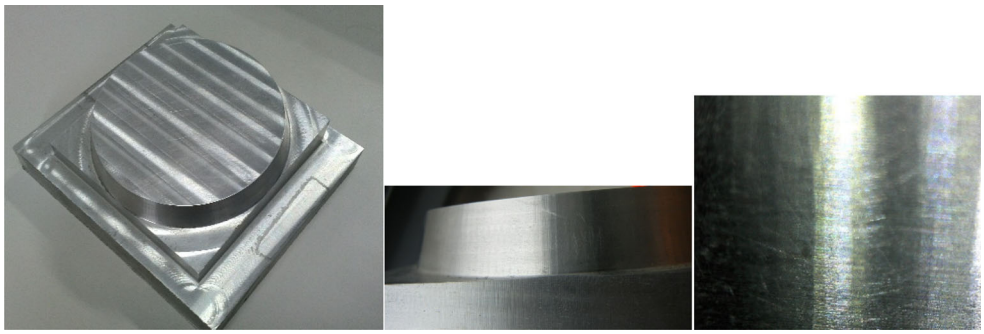

(a) (b) (c)

Fig. 30 Surface quality of NAS979 test piece machined by poor performance machine tool **a** The finished NAS979 test piece. **b** Surface of NAS979. **c** Surface detail of NAS979

NAS979 test piece is machined by the poor performance machine tool with the similar processing technique. The surface texture is display as shown in Fig. 30. The result of the machining NAS979 test piece shown in Fig. 30 is similar with the result of simulation. The machining quality of NAS979 is much better than 'S' test piece machined by the same machine tool.

Based on the comparative analysis of the experiment of 'S' test piece and NAS979, for the same performance servo system, the surface texture of the 'S' test piece could exhibit imperfect dynamic performance of the servo system than NAS979 more directly and intuitively. Because the surface textures of four special regions would degrade significantly with the performance of servo system, the shift in surface quality becomes obvious without the special equipment so that it is a convenient way to detect machine tool.

6 Conclusions

For the purpose to ensure the cause of surface morphology abnormality at machined 'S' test piece, the geometric and machining features of 'S' test piece have been analyzed. The discontinuity of the curvature of complex surface would require a higher performance five-axis machine tool to machine the 'S' test piece, and the changing of the speed and acceleration needs a better performance servo system. Then, a simulated platform is set up to amplify normal errors from tracking of axes. The simulation analysis of the unsmooth marks of 'S' test piece is performed. Then, the machining experiments of 'S' test piece are conducted under the suggested process. The result of the experiment is consistent with the simulation result, which means that the performance of servo system has direct influence on surface morphology abnormality. Finally, the comparative analysis of 'S' test piece and NAS979 is conducted. Both of the analysis results and experiment results show that the surface quality of 'S' test piece can exhibit the dynamic performance of the servo system of five-axis machine tool more directly than NAS979. Therefore, 'S' test piece can be used to improve the machining precision fast and convenient by the surface morphology state.

Acknowledgments This work is supported by 04 National Science and Technology Major Projects of China (2013ZX04001-021) and the National Science and Foundation of China (51205048).

References

1. Ye T, Xiong CH (2008) Geometric parameter optimization in multi-axis machining. Comput Aided Des 40(8):879–890
2. Schmitz TL, Ziegert JC, Canning JS, Zapata R (2008) Case study: a comparison of error sources in high-speed milling. Precision Eng J Int Soc Precis Eng Nanotechnol 32(2):126–133
3. ISO/CD 10791–6:2009 (2009) Test conditions for machining centers—part 6: accuracy of feeds, speeds and interpolations
4. Renishaw: http://www.renishaw.com
5. IBS Precision Engineering: http://www.ibspe.com
6. Fidia S.p.a.:http://www.fidia.it
7. NAS979 (1969) Uniform cutting test-NAS series, metal cutting equipment. NAS, USA
8. Song Z, Cui Y (2009) S-shape detection test piece and a detection method for detecting the precision of the numerical control milling machine. United States, Invention Patent, US8061052B2
9. Clarysse F, Vermeulen M (2004) Characterizing the surface waviness of steel sheet: reducing the assessment length by robust filtering. Wear 257(12):1219–1225
10. Al-Regib E, Ni J, Lee SH (2003) Programming spindle speed variation for machine tool chatter suppression. Int J Mach Tools Manuf 43(12):1229–1240
11. Gagnol V, Bouzgarrou BC, Ray P, Barra C (2007) Model-based chatter stability prediction for high-speed spindles. Int J Mach Tools Manuf 47(7–8):1176–1186
12. Ahmadi K, Ismail F (2010) Machining chatter in flank milling. Int J Mach Tools Manuf 50(1):75–85
13. Li ZZ, Zheng M, Zheng L, Wu ZJ, Liu DC (2003) A solid model-based milling process simulation and optimization system integrated with CAD/CAM. J Mater Process Technol 138(1–3):513–517
14. Bae SH, Ko K, Kim BH, Choi BK (2003) Automatic feedrate adjustment for pocket machining. Comput Aided Des 35(5):495–500
15. Guzel BU, Lazoglu I (2004) Increasing productivity in sculpture surface machining via off-line piecewise variable feedrate scheduling based on the force system model. Int J Mach Tools Manuf 44(1):21–28

16. Jiang L, Yahya E, Ding GF, Hu MH, Qin SF (2013) The research of surface waviness control method for 5-axis flank milling. Int J Adv Manuf Technol 69(1–4):835–847
17. Jung CY, Oh JH (1991) Improvement of surface waviness by cutting force control in milling. Int J Mach Tools Manuf 31(1):9–21
18. Luo X, Cheng K, Ward R (2005) The effects of machining process variables and tooling characterisation on the surface generation. Int J Adv Manuf Technol 25(11–12):1089–1097
19. Luo XK, Cheng K, Luo XC, Liu XW (2005) A simulated investigation on the machining instability and dynamic surface generation. Int J Adv Manuf Technol 26(7–8):718–725
20. Yamaguchi F (1988) Curves and surfaces in computer aided geometric design. Springer
21. Kato N, Tsutsumi M, Sato R (2013) Analysis of circular trajectory equivalent to cone-frustum milling in five-axis machining centers using motion simulator. Int J Mach Tools Manuf 64:1–11
22. Zhang LB, Wu T, Huang FL (2014) A coupling motional control method based on parametric predictive and variable universe fuzzy control for multi-axis CNC machine tools. Int J Adv Manuf Technol 74(5–8):1097–1114
23. ISO 12085. 1996 (1996) Geometrical Product Specifications (GPS)—surface texture: profile method—motif parameters